




# The inhibitory effects of mitragynine on P-glycoprotein in vitro

Noradliyanti Rusli<sup>1</sup> · Azimah Amanah<sup>2</sup> · Gurjeet Kaur<sup>3</sup> · Mohd Ilham Adenan<sup>4</sup> · Shaída Fariza Sulaiman<sup>5</sup> · Habibah Abdul Wahab<sup>6</sup> · Mei Lan Tan<sup>1,2</sup> 

Received: 14 August 2018 / Accepted: 14 December 2018 / Published online: 2 January 2019  
© Springer-Verlag GmbH Germany, part of Springer Nature 2019

## Abstract

Mitragynine is a major component isolated from *Mitragyna speciosa* Korth or kratom, a medicinal plant known for its opiate-like and euphoric properties. Multiple toxicity and fatal cases involving mitragynine or kratom have been reported but the underlying causes remain unclear. P-glycoprotein (P-gp) is a multidrug transporter which modulates the pharmacokinetics of xenobiotics and plays a key role in mediating drug-drug interactions. This study investigated the effects of mitragynine on P-gp transport activity, mRNA, and protein expression in Caco-2 cells using molecular docking, bidirectional assay, RT-qPCR, Western blot analysis, and immunocytochemistry techniques, respectively. Molecular docking simulation revealed that mitragynine interacts with important residues at the nucleotide binding domain (NBD) site of the P-gp structure but not with the residues from the substrate binding site. This was consistent with subsequent experimental work as mitragynine exhibited low permeability across the cell monolayer but inhibited digoxin transport at 10  $\mu$ M, similar to quinidine. The reduction of P-gp activity in vitro was further contributed by the downregulation of mRNA and protein expression of P-gp. In summary, mitragynine is likely a P-gp inhibitor in vitro but not a substrate. Hence, concurrent administration of mitragynine-containing kratom products with psychoactive drugs which are P-gp substrates may lead to clinically significant toxicity. Further clinical study to prove this point is needed.

**Keywords** *Mitragyna speciosa* Korth · Kratom · Mitragynine · P-glycoprotein · Bidirectional transport assay

## Introduction

Mitragynine is a primary psychoactive compound isolated from *Mitragyna speciosa* Korth (*M. speciosa*) and it is responsible for most of the plant's pharmacological activities. *M. speciosa*, or commonly known as kratom, belongs to the Rubiaceae family and has been traditionally used to manage various ailments such as cough, diarrhea, chronic pain, and drug withdrawal symptoms

(Chittrakarn et al. 2010; Jamil et al. 2013; Matsumoto et al. 2004). Kratom have opiate- and cocaine-like effects, hence, it has been frequently utilized as a stimulant or as a substitute for opiate addiction (Boyer et al. 2008; Grundmann 2017; Kong et al. 2011; Philipp et al. 2011). The narcotic, stimulant, and other dose-dependent effects of kratom have been attributed primarily to mitragynine (Matsumoto et al. 1996a; Matsumoto et al. 1996b; Thongpradichote et al. 1998).

**Electronic supplementary material** The online version of this article (<https://doi.org/10.1007/s00210-018-01605-y>) contains supplementary material, which is available to authorized users.

✉ Mei Lan Tan  
tanml@usm.my

<sup>1</sup> Advanced Medical & Dental Institute, Universiti Sains Malaysia, SAINS@BERTAM, Kepala Batas, Pulau Pinang, Malaysia

<sup>2</sup> Malaysian Institute of Pharmaceuticals & Nutraceuticals, National Institutes of Biotechnology Malaysia (NIBM), Ministry of Energy, Science, Technology, Environment and Climate Change (MESTECC), Georgetown, Pulau Pinang, Malaysia

<sup>3</sup> Institute for Research in Molecular Medicine (INFORMM), Universiti Sains Malaysia, Georgetown, Pulau Pinang, Malaysia

<sup>4</sup> Atta-ur-Rahman Institute for Natural Product Discovery, Universiti Teknologi MARA (UiTM), Shah Alam, Selangor Darul Ehsan, Malaysia

<sup>5</sup> School of Biological Sciences, Universiti Sains Malaysia, Penang, Pulau Pinang, Malaysia

<sup>6</sup> Pharmaceutical Drug Simulation Laboratory (PhDS), School of Pharmaceutical Sciences, Universiti Sains Malaysia, Georgetown, Pulau Pinang, Malaysia

Chronic usage of kratom has been associated with opioid abuse, dependence, and addiction. Despite listed as a regulatory controlled substance in Malaysia and Thailand, there is a rampant misuse of preparations containing kratom among the locals (Adkins et al. 2011; Hassan et al. 2013; Kapp et al. 2011). A majority of users admitted to daily consumption of kratom either by drinking in the form of tea, chewing, smoking, or adding the leaves to food (Ahmad and Aziz 2012; Swogger et al. 2015). There are currently no regulations to prohibit its use in some states in the United States of America (USA), United Kingdom (UK), and other countries (Boyer et al. 2008; Hillebrand et al. 2010; Schmidt et al. 2011). Although the US Drug Enforcement Agency in 2016 has announced plans to place kratom in Schedule 1 of the Controlled Substances Act, which would have effectively outlawed use of the product, the plans were shelved after a public outcry (Henningfield et al. 2018).

Self-treatment using kratom and co-administration of kratom with another herbal preparation or other drugs resulting in adverse reactions, toxicity, and deaths are often reported (Boyer et al. 2008; Domingo et al. 2017; Karinen et al. 2014; Kronstrand et al. 2011; Neerman et al. 2013; Nelsen et al. 2010; Tatum et al. 2018). Although mitragynine was discovered together with other substances during forensic analysis, the exact cause of toxicity or death remained largely uncertain. At least 36 deaths have been attributed to kratom so far, which prompted the Food and Drug Administration (USA) to issue a public health warning about the substance in November 2017 (White 2018). Kratom users usually have a previous drug history and often other psychoactive substances such as cannabis, heroin, and benzodiazepines were used concomitantly. The widespread use of mitragynine-containing kratom preparation certainly warrants safety precautions and investigations.

P-glycoprotein (P-gp) is a multidrug transporter and one of the members of the ATP-binding cassette (ABC) superfamily encoded by the *MDR1/ABCB1* gene in human (Hennessy and Spiers 2007). P-gp is synthesized in the endoplasmic reticulum as a core-glycosylated intermediate with a molecular weight of 150 kDa before subsequently modified in the Golgi apparatus prior to export to the surface of the cell (Grandjean-Forestier et al. 2009). P-gp protects cells from xenobiotics and toxins by pumping them out and the efflux of the components helps in preventing them from reaching the systemic circulation (Vaalburg et al. 2005). Due to its extreme broad substrate specificity and promiscuity, P-gp can actively transport a plethora of substrate compounds with varying size and structure out of the cells (Montanari and Ecker 2015; Pan et al. 2016). P-gp is mainly expressed along the apical (luminal) side of the epithelial cells of the intestine (enterocytes), brain capillary endothelial cells in blood brain barriers, and renal proximal tubular cells.

Transporters have the potential to impact oral bioavailability and modulates the absorption, distribution, and excretion

of a vast array of xenobiotics and serves a key role in drug-drug interactions (DDI) (Aszalos 2007; Borst and Elferink 2002; Szakacs et al. 2006; Vaalburg et al. 2005). Thus, alteration of enzyme and transporter activities of a substrate drug may lead to a reduction in drug efficacy or an induction of drug toxicity. For example, the presence of an inhibitor of P-gp may alter the bioavailability of a substrate drug in the intestine and has an impact on the clinical safety of the selected drug (Tachibana et al. 2010). Herb-induced P-gp inhibition and/or induction on its transport activity are potentially capable of changing the substrate drug's pharmacokinetic parameters and resulting in severe side effects or treatment failure.

Our previous study has reported that mitragynine is a weak CYP3A4 inhibitor. Although substrates and/or inhibitors of CYP3A4 and P-gp tend to overlap with each other, the effects of mitragynine on P-gp and the possibility of contributing to drug-herb interaction risks remain unclear and have not been fully explored. This study aims to determine the interactions between mitragynine and P-gp via molecular docking simulation and bidirectional assay. The effects of mitragynine on P-gp expression were also determined.

## Materials and methods

### Materials

Caco-2 cell line (ATCC® HTB-37) was obtained from the American Type Culture Collection (ATCC), USA. Minimum essential medium (MEM), fetal bovine serum (FBS), 0.05% (w/v) trypsin-EDTA, penicillin-streptomycin, and HEPES [4-(2-hydroxyethyl)piperazine-1-ethanesulfonic acid] solution were all from Gibco, USA. CellTiter 96® Aqueous one solution cell proliferation assay was obtained from Promega, USA. Modified Hank's balanced salt solution (HBSS), sodium acetate trihydrate, sodium pyruvate, MEM non-essential amino acid solution, dimethyl sulfoxide (DMSO), digoxin, quinidine, and rifampicin were all from Sigma-Aldrich, USA. QIAshredder™ and RNeasy® plus mini kit were from Qiagen, USA. Anti-MDR1/ABCB1 (E1Y7B) rabbit mAb, anti-human β-actin rabbit antibody, anti-rabbit IgH (H+L), F(ab')<sub>2</sub> fragment, anti-rabbit IgG HRP-linked antibody were purchased from Cell Signaling, USA. Ammonium persulfate, DC™ Protein assay reagent A and B, Precision Protein™ StrepTactin-HRP conjugate, Precision Plus Protein™ WesternC™ standard, and iTaq™ Universal SYBR® green one-step kit were all from Bio-Rad Laboratories Inc., USA. Taqman® RNA-to-CT™ 1-step kit and Mem-PER™ Plus membrane protein extraction kit was obtained from Thermo Scientific, USA. ECL™ Western blotting detection reagent is from GE Healthcare, UK. Acetonitrile and methanol gradient grade for liquid chromatography, sodium dodecyl sulfate (SDS), acrylamide/bis 30% (w/v), and molecular grade

ethanol were all purchased from Merck, Germany. Primers and probes were synthesized by Bioneer, Korea.

### Isolation and characterization of mitragynine

Mitragynine was isolated from *M. speciosa* Korth leaves and characterized as previously described (Lu et al. 2014; Tay et al. 2016). Briefly, the fresh leaves of the plant were collected from the state of Perlis, Malaysia, with written permission from the Ministry of Health Malaysia and the Narcotics Crime Investigation Department, Royal Malaysia Police (PDRM). The authentication work was carried out in Forest Research Institute Malaysia (FRIM) and specimen voucher code number IPHARM-49-35-C1 was deposited at the Malaysian Institute of Pharmaceuticals and Nutraceuticals (IPharm). Briefly, powdered dried material was extracted with methanol for 72 h using Soxhlet apparatus to obtain methanol extract. The extract was subsequently dissolved in 10% (v/v) acetic acid to yield the acidic filtrate. The filtrate was first washed with n-hexane and 25% (v/v) ammonia solution before extracted with chloroform and subsequently processed with anhydrous sodium sulfate to produce the crude alkaloid extract. Subsequently, the crude alkaloid was fractionated with n-hexane and ethyl acetate eluent system and fractions were subjected to preparative TLC to increase the purity of the compound. Further recrystallization was carried out with n-hexane and diethyl ether to produce an approximately 30% (w/w) of mitragynine. The structure and identity of the compounds were confirmed using <sup>1</sup>H-NMR and <sup>13</sup>C-NMR analysis as shown in Supplementary Fig. 1 (Lu et al. 2014).

### Molecular docking

The structures of digoxin, quinidine, and mitragynine were constructed using ACD/ChemSketch Freeware (Advanced Chemistry Development, INC., Toronto, ON, Canada) and optimized using PRODRG server (<http://davapc1.bioch.dundee.ac.uk/prodrg/>). The three-dimensional structure of P-gp was downloaded from the RCSB Protein Data Bank as a protein databank file (PDB Code: 4KSB) (Ward et al. 2013). Molecular docking simulation was carried out using AutoDock 4.2.6 software package (Morris et al. 2009), whereas the docking files were prepared using the AutoDockTools (ADT) 1.5.6 RC3 package. A grid map of 126 × 126 × 126 points in x, y, z-direction with a spacing of 0.375 Å between the grid points was set. The Lamarckian genetic algorithm (LGA) was used for the ligand conformational search and 100 independent docking runs were made. The 100 docked conformations of the ligands were clustered based on a root mean square deviation (RMSD) tolerance of 2.0 Å. The molecular interactions of the ligands with P-gp were analyzed using Accelrys® Discovery Studio 4.0 (Accelrys, Inc., USA). Parameters such as free energy of binding (FEB),

estimated inhibition constant ( $K_i$ ), and important residues of macromolecule binding site were compared with digoxin (substrate) and quinidine (inhibitor) as reference controls.

### Cell culture and cell proliferation assay

Caco-2 cell line was maintained in MEM supplemented with 1% (v/v) sodium pyruvate, 1% (v/v) non-essential amino acid, 100 U/mL of penicillin and 100 µg/mL of streptomycin (also known as complete MEM), and 10% (v/v) FBS at 37 °C in a humidified incubator supplemented with 5% (v/v) CO<sub>2</sub>. For all the experiments, cells from different passage numbers were used in each independent experiment carried out on different days. Briefly, cells were seeded onto two 96-well plates (Nunc, Denmark) with an optimized number of approximately 6000 cells per well and were allowed to grow for 24 h. After 24 h, cells in T<sub>0</sub> plate were subjected to cell proliferation assay while cells in T<sub>1</sub> plate were cultured in a reduced serum medium containing 0.5% (v/v) FBS-complete MEM for 4 h. Subsequently, medium in T<sub>1</sub> plate was replaced with reduced serum medium containing drug/compound and incubated for 72 h. Control cells were treated with 0.1% (v/v) of DMSO (vehicle) in 0.5% (v/v) FBS-complete MEM. Cell proliferation assay was carried out using CellTiter 96® AQ<sub>UCOUS</sub> one solution cell proliferation assay reagent (Promega, USA) following the manufacturer's protocol. Percentage of growth and response parameters were calculated as previously described (Tan et al. 2016).

### Bidirectional transport assay

Briefly, for bidirectional transport assay, Caco-2 cells were seeded onto Transwell® polycarbonate membrane cell culture insert (6.5 mm; 0.4 µm pore size) (Corning, USA) placed in a 24-well plate with a density of approximately 1 × 10<sup>5</sup> cells/cm<sup>2</sup> per insert and allowed to grow according to the manufacturer's instructions. On the third day of culture, the medium was replaced with complete MEM without FBS on the apical side and 10% (v/v) FBS-complete MEM on the basolateral side for differentiation of the cells to mimic intestinal condition (Ferruzza et al. 2012). The medium was changed every 2 days until 21 days of culture prior to bidirectional assay (Peng et al. 2014). To measure the integrity of the cell membrane, the transepithelial electrical resistance (TEER) values were monitored in each well using Millicell® ERS-2 Voltohmmeter (Milipore, Germany). The TEER values were calculated from the resistance readings recorded on 7th, 14th, and 21st days of the cells cultured in the membrane insert using the following formula, where TEER value = (resistance of sample – resistance of blank) × effective membrane area (Srinivasan et al. 2015). Cell monolayers with TEER values between 350 and 600 Ωcm<sup>2</sup> were used for subsequent assays.

For P-gp substrate determination, cells were first pre-incubated with transport buffer [modified HBSS with 10 mM HEPES (pH 7.4)] on the apical and basolateral side of the membrane insert, respectively for 20 min at 37 °C. Subsequently, the buffer was replaced with freshly prepared compound diluted in complete transport buffer into the apical side and transport buffer into the basolateral side to measure the transport of compound from apical to basolateral. To measure the transport of compound from basolateral to apical side, compound solution was added into the basolateral side instead. The cells were then incubated at 37 °C and the samples were collected at an optimized time of 210 min, which was the linear phase in the permeability. For the measurement of the transport of compound from apical to the basolateral (AP-BL) side, sample solution was taken from the basolateral chamber while for the measurement of the transport of compound from basolateral to apical (BL-AP) side, sample solution was taken from the apical chamber. The concentrations of the compound in the chambers were determined using HPLC analysis. The apparent permeability coefficient ( $P_{app}$ ) and net efflux ratio (ER) were calculated based on the final concentration of the drug at the receiver chamber (Mikkaichi et al. 2014; Oga et al. 2012). To confirm the functionality of the bidirectional assay, transport of digoxin (10  $\mu$ M) was first evaluated in the absence and presence of quinidine, a P-gp inhibitor (Wang et al. 2008).

As for P-gp inhibition studies, cells were grown on the insert as mentioned previously and were allowed to differentiate into polarized endothelial cells for 21 days. On day 18, cells were first pre-treated with compound for 72 h (Haslam et al. 2008). On day 21, cells were rinsed and pre-incubated in transport buffer for 20 min at 37 °C before incubated with mixture containing 10  $\mu$ M digoxin and a specific concentration of drug/compound in transport buffer at the apical side and transport buffer without digoxin at the basolateral chamber. To measure the transport of digoxin from BL-AP side in the presence of compound, digoxin in the presence of compound diluted in transport buffer was added into the basolateral side and transport buffer without digoxin was added into the apical side. The cells were then incubated and the sample solutions collected from the receiver chamber were analyzed as previously mentioned. Rifampicin (10  $\mu$ M) and quinidine (10  $\mu$ M) were used as controls for inducer and inhibitor respectively.

### HPLC analysis

Both digoxin and mitragynine samples were analyzed using Waters Breeze™ High Performance Liquid Chromatography (HPLC) system (Milford, MA, USA) equipped with Waters 1525 binary HPLC pump, Waters 717 Plus autosampler, and Waters 2487 dual  $\lambda$  absorbance detector. System operation and data acquisition was controlled using the Breeze™ software (Version 3.3). Chromatographic separation for digoxin

was performed using XBridge™ C18 Column with particle size of 5  $\mu$ m and a dimension of 150 mm  $\times$  3.0 mm as labeled by the manufacturer (Waters, Milford, MA, USA). For each injection, 100  $\mu$ L of sample was injected and peaks were monitored using ultraviolet detector at the wavelength of 220 nm. Samples were analyzed with isocratic elution system using HPLC mobile phase consisted of 72% (v/v) ultrapure water and 28% (v/v) acetonitrile with a flow rate of 0.5 mL/min and for 15 min (Jedlička et al. 2003; Varma et al. 2004). On the other hand, chromatographic separation for mitragynine was carried out using Zorbax StableBond C18 Column with particle size of 5  $\mu$ m and dimension of 250 mm  $\times$  3.0 mm as labeled by the manufacturer (Agilent Technologies, Santa Clara, CA, USA). For each injection, 20  $\mu$ L of sample was injected and peaks were monitored using ultraviolet detector at wavelength of 225 nm. Samples were analyzed using HPLC mobile phase consisted of 30% (v/v) acetate buffer and 70% (v/v) methanol with a flow rate of 0.8 mL/min and for 15 min (Janchawee et al. 2007; Lim et al. 2013). Retention time for drug/compound and bio-analytical method validation comprising selectivity, linearity, between- and within-day precision, and accuracy were determined prior to bidirectional assay. The concentration of drug/compound in sample solutions was calculated by reference to a standard curve constructed from known concentrations of the drug/compound.

### Reverse transcription-quantitative real-time PCR (RT-qPCR)

Briefly, cells were first seeded into T25 flasks with an optimum density and were allowed to grow until 70% confluence. Subsequently, the medium was replaced with 0.5% (v/v) FBS-complete MEM and incubated for 4 h prior to treatment with drug/compound for the next 72 h. Total RNA was isolated from the treated cells using QIAshredder™ and RNeasy® plus mini kit (Qiagen, Germany) according to manufacturer's protocol. All primers and probes were designed using Beacon Designer 7.80 (Premier Biosoft International, USA) (Table 1). To determine the optimum annealing temperature for each set of primers, gradient RT-qPCR was carried out using iTaq™ Universal SYBR® Green One-Step kit (Bio-Rad Laboratories, USA). To optimize the concentration of the probes and in subsequent experiments, RT-qPCR was carried out using Taqman® RNA-to-CT™ 1-Step Kit (Thermo Scientific, USA) in CFX96™ real-time PCR detection system (Bio-Rad Laboratories, USA). The thermal profile used for amplification was as follows: cycle 1 (cDNA synthesis), consisting of 15 min at 48.0 °C; cycle 2 (reverse transcriptase inactivation), consisting of 10 min at 95.0 °C; cycle 3 (PCR), consisting of 15 s at 95.0 °C followed by 1 min at 56.3 °C for 40 cycles; and cycle 4



**Table 1** Oligonucleotide primer and probe sets used for the PCR analysis

Gene	Sequences
MDR/ABCB1/P-gp	
Forward	5' – TGCCTATTATTACAGTGGAA – 3'
Reverse	5' – TCTCCTGTGCGCATTATAG – 3'
Probe	FAM-TGCTGGTTGCTGCTTACATTCA-EBQ
$\beta$ -actin	
Forward	5' – ATCACCATTGGCAATGAG – 3'
Reverse	5' – GATGGAGTTGAAGGTAGTT – 3'
Probe	Cy5-CACTCTTCCAGCCTTCCTTCC-BHQ 2
GAPDH	
Forward	5' – ATTCCACCCATGGCAAATTC – 3'
Reverse	5' – GATGGGATTTCATTGATGACA – 3'
Probe	HEX-CCGTTCTCAGCCTTGACGGTGC-BHQ1

(melt curve analysis), consisting of 5 s at 65–95 °C for 60 cycles, increasing by 0.5 °C for each cycle. The RT-qPCR amplification efficiency for each set of primers was determined and computed into the Pfaffl mathematical model for subsequent calculation of relative gene expression. Data are presented as the fold change in gene expression normalized to two endogenous reference genes (GAPDH and  $\beta$ -actin) and relative to the vehicle-treated control. Caco-2 cells incubated with 0.1% (v/v) DMSO in 0.5% (v/v) FBS-complete MEM for 72 h was used as vehicle control. The final concentration of DMSO in all treatment conditions did not exceed 0.1% (v/v).

### Western blot analysis

Caco-2 cells were seeded into T75 flask with an optimum density and were treated with drug/compound as mentioned previously. Total membrane protein was isolated using Mem-PER™ Plus membrane protein extraction kit (Thermo Scientific, USA). The proteins were then separated by SDS-PAGE and electrophoretically transferred to the PVDF membrane using Mini Trans-Blot® electrophoretic transfer cell (Bio-Rad Laboratories, USA) according to the manufacturer's protocol. After blocking with 3% (w/v) skim milk in PBS-T, the membranes were probed with an optimized dilution of primary antibodies overnight (1:1000 for both anti-MDR1/ABCB1 (E1Y7B) rabbit mAb and anti-human  $\beta$ -actin rabbit antibody) and finally incubated with IgG HRP-linked secondary antibody (Cell Signaling Technology, USA) (1:1000) for 2.5 h. The signal was detected using ECL™ Western blotting detection reagents (Amersham Biosciences, UK) and imaged on ChemiDoc™ XRS imaging system (Bio-Rad Laboratories, USA). Densitometric quantification of the bands was performed using the Image Lab™ analysis

software (Bio-Rad Laboratories, USA). Protein expression was normalized against  $\beta$ -actin, which served as internal control of protein loading. Relative protein expression was then calculated by dividing the normalized intensity of treated sample by vehicle control.

### Immunocytochemistry

Briefly, the Caco-2 cells were seeded onto 12-well plates with Transwell® polycarbonate membrane inserts (Corning, USA) with an approximate density of  $1 \times 10^5$  cells/cm<sup>2</sup>. The cells were allowed to grow and after 3 days, the complete medium was changed to medium without FBS on the apical side and 10% (v/v) FBS-complete medium on the basolateral side (Ferruzza et al. 2012). The next day, the previous medium was replaced with drug/compound diluted in complete medium without FBS in the apical side and 10% (v/v) FBS-complete medium in the basolateral chamber. The monolayer cell was further incubated for 72 h before fixation and staining for confocal microscopy. Monolayer cells were fixed with 4% (v/v) paraformaldehyde and incubated for 30 min at room temperature followed by permeabilization using 0.1% (v/v) Triton X-100 for 15 min and blocking with 3% (v/v) bovine serum albumin for 1 h. The cells were then incubated with an optimized dilution of anti-MDR1/ABCB1 (E1Y7B) rabbit mAb (Cell Signaling, USA) (1:800) in 3% (v/v) BSA and incubated at 4 °C overnight. Subsequently, cells were rinsed with PBS-T and incubated with anti-rabbit IgG (H+L), F(ab')<sub>2</sub> Fragment (Alexa Fluor® 488 conjugate, Cell Signaling, USA) at optimized dilution (1:1000) in 3% (v/v) BSA for 1 h. Finally, the polycarbonate membrane was detached from the insert and carefully placed onto a glass slide and mounted with Fluoroshield™ with DAPI mounting medium (Sigma, USA) and flipped it with the cells facing downwards before viewing under 63× objective magnification using Nikon C2 confocal microscope (Nikon, USA). The excitation/emission wavelengths for Alexa-488 and DAPI were 490/525 nm and 358/461 nm, respectively. The settings for laser imaging including laser power, gain and amplification factor were set similarly for all slides. For each independent experiment, ten spots (image at 63× objective magnification) with approximately 100 cells per spot were randomly selected for each slide. The integrated density of the green fluorescence (Alexa Fluor® 488) of the confocal images was measured using the ImageJ software (<http://imagej.nih.gov/ij/>). From the ImageJ analysis, the relative protein expression was calculated by dividing the density values of treated cells relative to the control cells (0.1% (v/v) DMSO). In addition to the densitometry analysis, the percentage numbers of cells expressing the protein were also selected and quantified.

## Data analysis

The permeability coefficient ( $P_{app}$ ) and ER of the compounds were calculated using the following equations:

$$P_{app} = \frac{1}{C_0 A} \frac{dQ}{dt}$$

where  $dQ/dt$  is the steady-state appearance rate of the substrate on the receiver side (dpm/s),  $C_0$  is concentration of the test compound on the donor side (dpm/ $\mu$ L), and  $A$  is the surface area of the monolayer (0.33  $\text{cm}^2$ ) (Mikkaichi et al. 2014).

$$ER = \frac{P_{app \text{ BL-AP}}}{P_{app \text{ AP-BL}}}$$

$P_{app \text{ BL-AP}}$  is the  $P_{app}$  value from the basal to apical direction and  $P_{app \text{ AP-BL}}$  is the  $P_{app}$  value from the apical to basal direction. Statistical comparisons were performed using unpaired Student's  $t$  test and results were expressed as means  $\pm$  SD of three independent experiments (GraphPad Prism® software, version 5.0). Results are considered statistically significant if  $p$  value  $< 0.05$ .

## Results

### Molecular docking of mitragynine within the P-gp substrate and NBD-binding site

To investigate the interactions between compounds and the drug binding sites of P-gp, parameters such as free energy of binding (FEB), estimated inhibition constant ( $K_i$ ) and interactions with important residues within P-gp were evaluated. Based on the docking simulation of mitragynine and digoxin within the substrate binding site of P-gp, mitragynine was demonstrated to have a higher calculated FEB ( $-6.69$  kcal/mol) and  $K_i$  (12.53  $\mu$ M) values as compared with digoxin ( $-7.77$  kcal/mol; 2.01  $\mu$ M) (Table 2). As a known substrate, digoxin forms a single hydrogen bond with Tyr303 residue and hydrophobic interactions with some of the important substrate binding site residues of P-gp (Fig. 1a). The methyl group of digoxin forms  $\pi$ -sigma interaction with the pi-orbitals of the benzene ring of the aromatic residue of Tyr306 whereas the alkyl group forms  $\pi$ -alkyl interactions with  $\pi$ -orbitals of the benzene ring of the aromatic residues of Tyr303, Phe339, Phe724, Tyr949, and Phe974. Digoxin also forms alkyl to alkyl hydrophobic interactions with P-gp residues such as

**Table 2** Molecular interaction of mitragynine within the substrate binding site and the nucleotide binding domain (NBD) of P-gp

Compound		Substrate binding site of P-gp				Free energy binding, FEB (kcal/mol)	Estimated inhibition constant, $K_i$ ( $\mu$ M)
		Hydrogen bonding		Hydrophobic interactions			
		Important residues	Others	Important residues	Others		
Known substrate	Digoxin	Tyr303 ( $\surd$ )		Tyr303 (2 $\pi$ -alkyl), Tyr306 ( $\pi$ -sigma), Phe339 (2 $\pi$ -alkyl), Phe724 ( $\pi$ -alkyl), Tyr949 ( $\pi$ -alkyl), Phe974 ( $\pi$ -alkyl), Ile977 (alkyl-alkyl), Val978 (3 alkyl-alkyl)	Ile302 (3 alkyl-alkyl), Ala981 (alkyl-alkyl)	$-7.77$	2.01
Natural compound	Mitragynine		Gly826 ( $\surd$ ), Phe833 ( $\surd$ )		Ala714 ( $\pi$ -alkyl), Phe766 ( $\pi$ - $\pi$ T-shaped), Phe773 ( $\pi$ - $\pi$ stacked), Leu829 (amide- $\pi$ stacked, $\pi$ -alkyl), Ala830 (amide- $\pi$ stacked, 2 $\pi$ -alkyl)	$-6.69$	12.53
Compound		Nucleotide binding domain (NBD) of P-gp				Free energy binding, FEB (kcal/mol)	Estimated inhibition constant, $K_i$ ( $\mu$ M)
		Hydrogen bonding		Hydrophobic interactions			
		Arg258	Others	Pro803	Others		
Known inhibitor	Quinidine	$\surd$	Phe800 ( $\surd\surd$ )	alkyl-alkyl	Arg258 (2 $\pi$ -alkyl), Leu810 (alkyl-alkyl)	$-7.57$	2.83
Natural compound	Mitragynine	$\surd\surd\surd$	Asp801 ( $\surd$ ), Asp802 ( $\surd$ ), Pro803 ( $\surd$ ), Asn805 ( $\surd$ ), Gln1077 ( $\surd\surd$ )	2 $\pi$ -alkyl	Tyr1040 ( $\pi$ -alkyl)	$-7.05$	7.76

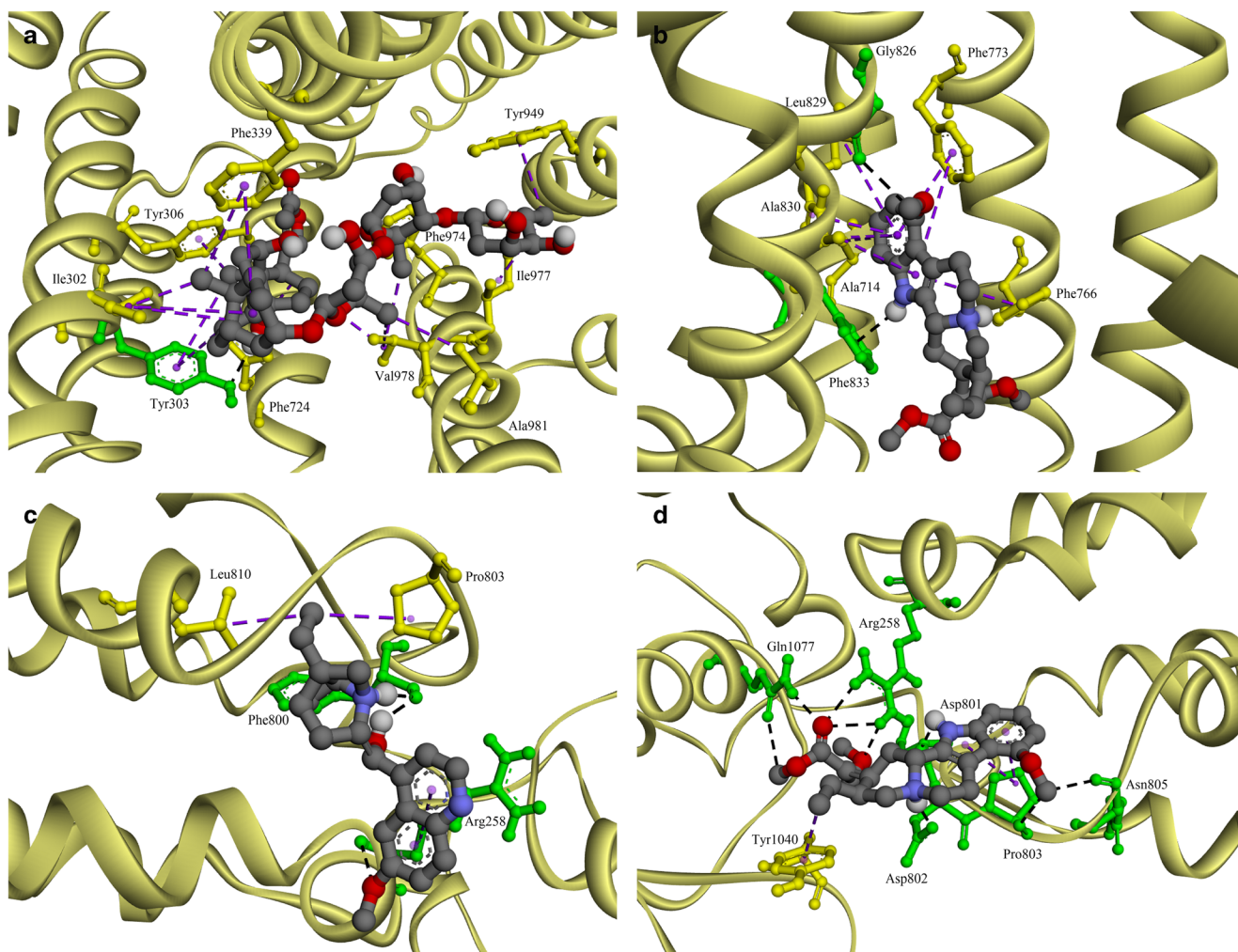


**Fig. 1** Detailed molecular interaction between compound and substrate binding site and nucleotide binding domain (NBD) of P-gp. **a** Digoxin and substrate binding site. **b** Mitragynine and substrate binding site. **c** Quinidine and NBD. **d** Mitragynine and NBD. The conformations of ligands are shown in ball and stick representation. Atoms were colored

as gray for carbon, blue for nitrogen, red for oxygen, and white for hydrogen. The hydrophobic interactions and hydrogen bonds are depicted by purple and black lines meanwhile P-gp residues which interact with compound by either hydrophobic interactions or hydrogen bond are represented by yellow or green structures respectively

Ile302, Ile977, Val978, and Ala981 (Fig. 1a). However, mitragynine did not have any form of interactions with the above residues. Mitragynine forms two hydrogen bonds with residues such as Gly826 and Phe833 (Fig. 1b). It also forms  $\pi$ - $\pi$  interactions ( $\pi$ - $\pi$  stacked and  $\pi$ - $\pi$  T-shaped) with the pi-orbitals of the benzene ring of the aromatic residues of Phe773 and Phe766 and  $\pi$ -alkyl interactions with residues such as Ala830, Ala714, and Leu829. In addition, Leu829 and Ala830 also form amide- $\pi$  stacked interactions with mitragynine. Based on this molecular docking simulation, mitragynine did not form any interactions with important residues of the substrate binding site of P-gp (Tyr303, Tyr306, Phe339, Phe724, Tyr949, Phe974, Ile977, Val978). These findings suggest that mitragynine may be a poor or non-P-gp substrate.

For prediction of P-gp inhibitor, based on the compound-P-gp complex interactions, mitragynine ( $-7.05$  kcal/mol)

appeared to be a slightly weaker inhibitor as compared with quinidine ( $-7.57$  kcal/mol) (Table 2). In addition, the  $K_i$  value of mitragynine ( $7.76$   $\mu$ M) was also higher as compared with quinidine ( $2.83$   $\mu$ M). From the docking simulation, both quinidine and mitragynine form hydrogen bonds with Arg258 residue of the P-gp (single hydrogen bond with quinidine, multiple hydrogen bonds with mitragynine). Quinidine forms additional two hydrogen bonds with Phe800 residue, whereas mitragynine has additional two hydrogen bonds with Gln1077 and single hydrogen bonds with Asp801, Asp802, Pro803, and Asn805 residues respectively (Fig. 1c, d). As for hydrophobic interactions, the alkyl group of quinidine form an alkyl to alkyl hydrophobic interactions, whereas the pi-orbitals group of mitragynine forms two  $\pi$ -alkyl interactions with Pro803 residues of P-gp. In quinidine, two additional  $\pi$ -alkyl interactions were seen between the pi-orbitals of quinidine and the alkyl groups of Arg258. Another alkyl to alkyl

hydrophobic interaction was also observed between the alkyl groups of quinidine with the alkyl group of Leu810 residue. On the other hand, the alkyl group of mitragynine forms additional hydrophobic interaction with the pi-orbitals of Tyr1040. Surprisingly, based on these molecular docking simulation, mitragynine and quinidine formed both hydrogen bonds and hydrophobic interactions with the same residues of P-gp (Arg258 and Pro803). Thus, there is a possibility that mitragynine may act as an inhibitor of P-gp, similarly to quinidine.

### The concentration testing range for mitragynine and optimization of the bidirectional transport assay

The possible cytotoxicity effects of mitragynine on Caco-2 cell line were determined at 72 h. The  $IC_{50}$  (50% growth inhibition), TGI (total growth inhibition), and  $LC_{50}$  (50% lethal concentration) values were calculated from a nonlinear regression model (curvefit) of sigmoidal dose-response curve using GraphPad Prism 5 (GraphPad Software, Inc., USA). Based on the interpolated values, the  $IC_{50}$ , TGI, and  $LC_{50}$  values of mitragynine were determined as 20.0, 56.20, and 112.20  $\mu\text{M}$  respectively, which were all higher as compared with the control drug (Supplementary Fig. 2a). Thus, mitragynine concentration range (0.001–10  $\mu\text{M}$ ) not exceeding  $IC_{50}$  value was used in subsequent experiments. Concentrations above 10  $\mu\text{M}$  may inhibit the growth and affect the P-gp transport activity of the Caco-2 cells.

Chromatographic retention time for compounds and HPLC method validation comprising selectivity, linearity, within- and between-day precision, and accuracy were first determined prior to bidirectional assay. The min retention time of mitragynine and digoxin was determined at 6.2 min and 5.9 min, respectively (Supplementary Fig. 2b, c). As for HPLC method validation, there was no interfering peak from the blank mixture during the retention time determination for both compounds indicating the selectivity of the chromatographic separation procedures. Both mitragynine and digoxin also produce a linear response over the tested concentration range and the coefficients of determination ( $R^2$ ) of both compounds were calculated as 1.000 as evidence of acceptable fit of the data to the regression line (Supplementary Fig. 2d, e). The within-day and between-day precision (% RSD) and accuracy (% RE) data for digoxin and mitragynine were all within the acceptance criteria of 20%.

The bidirectional transport assay was first validated using digoxin, with and without the presence of P-gp inhibitor (10  $\mu\text{M}$  of quinidine). In this assay, digoxin, a well characterized P-gp probe showed vectorial transport ( $P_{\text{app AP-BL}} < P_{\text{app BL-AP}}$ ), with an approximately 10-fold of  $P_{\text{app BL-AP}}$  value of  $(51.83 \pm 0.07) \times 10^{-6}$  cm/s as compared with  $P_{\text{app AP-BL}}$  value of  $(5.40 \pm 0.00) \times 10^{-6}$  cm/s, indicating significant expression of P-gp at the apical side of Caco-2 monolayer cell (Supplementary Fig. 2f).

The ER ( $P_{\text{app BL-AP}}/P_{\text{app AP-BL}}$ ) value of digoxin was calculated to be  $9.60 \pm 0.01$ . Unsurprisingly, in the presence of quinidine at both AP and BL sides, the  $P_{\text{app BL-AP}}$  was reduced to  $(23.50 \pm 0.30) \times 10^{-6}$  cm/s, while  $P_{\text{app AP-BL}}$  remained unchanged [ $(5.40 \pm 0.00) \times 10^{-6}$  cm/s]. Although the values for  $P_{\text{app AP-BL}}$  in the presence of inhibitor are expected to be different from the values without the inhibitor, the differences were not detected, probably due to the moderate to low sensitivity of the HPLC system. A clear reduction in the ER was observed for digoxin from  $9.60 \pm 0.01$  (without quinidine) to  $4.35 \pm 0.04$  (with quinidine) indicating inhibition of the transport activity and the functionality of the monolayer cells in the bidirectional assay.

### Mitragynine has minimal permeability but inhibits the transport of digoxin across the cell membrane

Permeability of mitragynine across P-gp-over expression Caco-2 cells was monitored as mentioned previously. Figure 2a shows  $P_{\text{app}}$  and ER values of mitragynine across Caco-2 monolayer cell with digoxin as control substrate. Interestingly, the  $P_{\text{app BL-AP}}$  value of mitragynine [ $(17.70 \pm 0.00) \times 10^{-6}$  cm/s] was rather similar compared with the  $P_{\text{app AP-BL}}$  [ $(18.83 \pm 0.87) \times 10^{-6}$  cm/s], indicating passive transport. This was in contrary to digoxin, where  $P_{\text{app BL-AP}}$  was much higher as compared with the  $P_{\text{app AP-BL}}$  and the ER value was near 10-fold. In the presence of quinidine, the  $P_{\text{app BL-AP}}$  of digoxin was significantly reduced but not for mitragynine (Fig. 2a). Mitragynine exhibited minimal permeability and appeared to be a poor P-gp substrate with ER value of  $0.94 \pm 0.04$  ( $< 2$ ).

The effects of mitragynine on the P-gp transport activity of digoxin was carried out subsequently. As shown in Fig. 2b, c, the mean ER values of digoxin in the presence of 0.1  $\mu\text{M}$ , 1  $\mu\text{M}$ , and 10  $\mu\text{M}$  of mitragynine were  $21.41 \pm 0.62$ ,  $18.26 \pm 1.67$ , and  $12.48 \pm 0.42$  respectively, indicating the transport of digoxin in the BL-AP direction was reduced with increasing concentration of mitragynine and suggesting a reduction in P-gp transport activity. However, only higher concentration of mitragynine (10  $\mu\text{M}$ ) produced a significant inhibition on the  $P_{\text{app BL-AP}}$  [ $(37.23 \pm 2.48) \times 10^{-6}$  cm/s] and reduction of ER value of digoxin (30%) as compared with the control experiment. Surprisingly, at the lowest concentration, there was a slight but significant induction of  $P_{\text{app BL-AP}}$  and ER values as compared with baseline. As expected, 10  $\mu\text{M}$  of quinidine showed a significant reduction in the digoxin transport with  $P_{\text{app BL-AP}}$  of  $(32.42 \pm 1.19) \times 10^{-6}$  cm/s and ER value of  $10.62 \pm 1.17$  (40% reduction) while rifampicin produced a significant induction with an ER value of  $19.65 \pm 0.90$ .

### Mitragynine downregulates the mRNA and protein expression of P-gp

To determine the effects of mitragynine on the gene expression of P-gp in Caco-2 cell line, RT-qPCR were carried out.



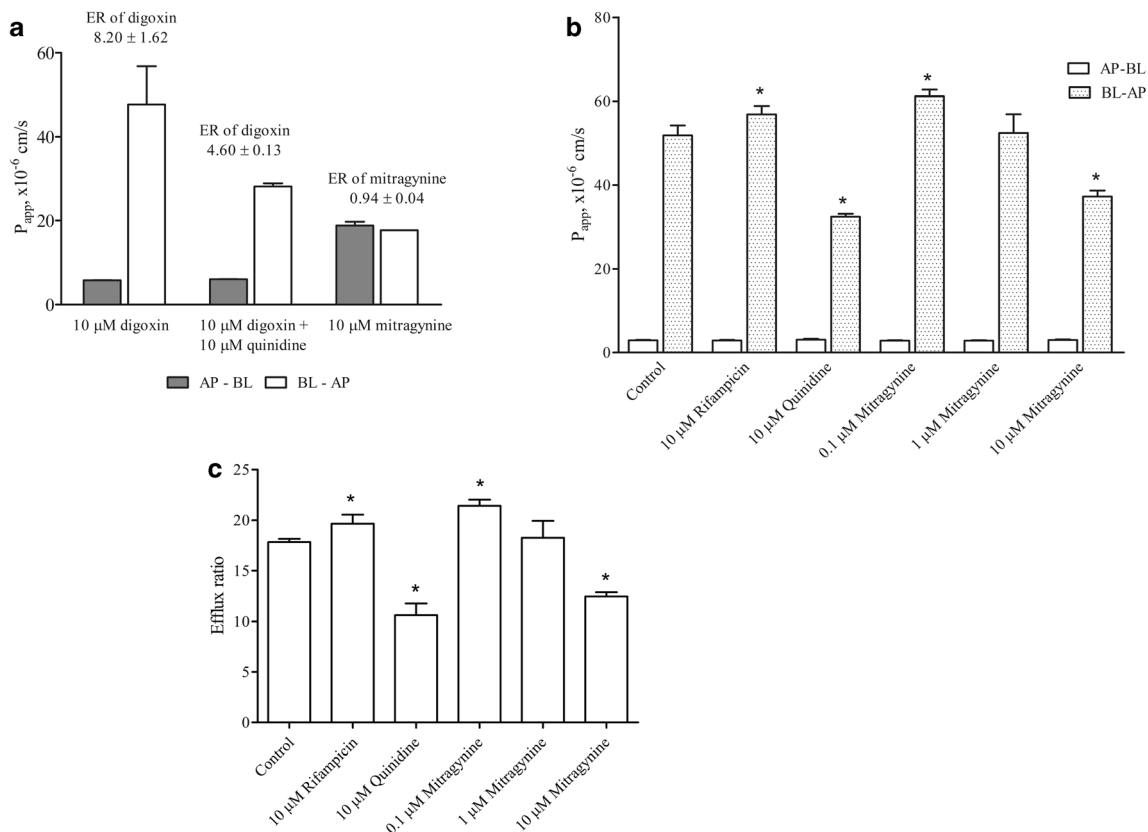


**Fig. 2** **a** Permeability of mitragynine across Caco-2 monolayer cells with digoxin as control. **b**  $P_{app}$  values of digoxin in the presence and absence of mitragynine and control drugs. **c** ER values of digoxin in the presence

and absence of mitragynine and control drugs. Data are presented as mean value  $\pm$  SD of three independent experiments ( $n = 3$ , \* $p < 0.05$  compared with control)

Figure 3a shows that mitragynine downregulated the mRNA expression of P-gp in a concentration-dependent manner, where a significant reduction was observed at 1 and 10  $\mu$ M (35.2% reduction; 1.54-fold at 10  $\mu$ M). Concentrations at 0.1  $\mu$ M and less did not produce any significant effects on the mRNA expression of P-gp. The mRNA results were in agreement with the protein expression pattern as the P-gp protein expression were also reduced in a concentration-dependent manner (Fig. 4a). For Western analysis, two bands were seen between 150 and 250 kDa and densitometry analysis of the upper band was determined as it was assumed to be the glycosylated membrane protein. The highest and significant inhibition occurred at 10  $\mu$ M with 39.4% (1.65-fold) inhibition, whereas 1  $\mu$ M of mitragynine showed 26.3% (1.36-fold) inhibition. The significant down-regulation of both P-gp mRNA and protein expression were consistent with the decrease in the net digoxin efflux ratio.

As a control inhibitor of digoxin transport, quinidine showed a concentration-dependent mRNA inhibition with the highest fold inhibition at 10  $\mu$ M [76.8%; 4.35-fold] (Fig. 3b). Although concentrations lower than 10  $\mu$ M generally produced more than 2-fold reduction in mRNA expression, the reduction was statistically insignificant ( $p > 0.05$ ). On the other hand, statistically significant protein downregulation was only observed

in cells treated with 1  $\mu$ M of quinidine (Fig. 4b). Interestingly, no clear pattern can be seen with increasing concentration of rifampicin as shown in Fig. 3c. The highest mRNA induction was seen at 10  $\mu$ M with 32.2% induction (1.32-fold) but none of these changes were statistically significant. On the other hand, P-gp protein expression was found to be increased in concentration-dependent manner where 10  $\mu$ M of rifampicin showed 99.8% (2.00-fold) induction while other lower concentrations showed 60.2% (1.60-fold), 42.0% (1.42-fold), 36.3% (1.36-fold), and 19.4% (1.19-fold) induction respectively (Fig. 4c). As a P-gp inducer, rifampicin significantly induced the protein expression of P-gp at all concentrations tested.

### Mitragynine reduces the localization of P-gp on the cell membrane

To identify the effects of mitragynine on the protein expression of P-gp on the surface of the cells, immunocytochemistry was carried out. From the cross-sectional view of Caco-2 cells, P-gp was found to be localized on the apical side of the cells. Generally, green fluorescence dots were seen on the membrane of the Caco-2 cells, while none was found on the cytoplasm. The fluorescence intensity of mitragynine-treated cells was the lowest when the concentration used was the highest (Figs. 5 and

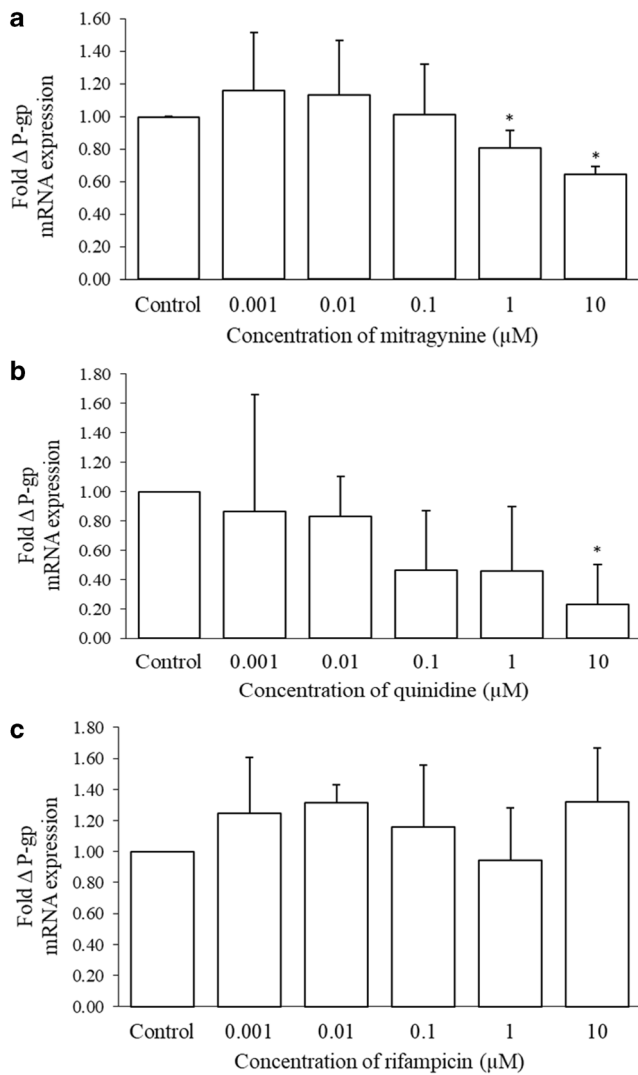


**Fig. 3** The effects of (a) mitragynine (b) quinidine (c) rifampicin on the mRNA expression of P-gp after 72 h of treatment. Data are presented as mean  $\pm$  SD of three independent experiments ( $n = 3$ , \* $p < 0.05$  compared with control)

6). As for controls, greater intensity of the green fluorescence was observed in cells treated with rifampicin while the lowest intensity was seen in quinidine-treated cells. Mitragynine inhibited the P-gp protein expression significantly in a concentration-dependent manner with more than 2-fold reductions for concentrations of 1  $\mu$ M (53.8%; 2.16-fold) and 10  $\mu$ M (64.8%; 2.84-fold) (Fig. 5a). Mitragynine was also found to significantly reduce the percentage number of cells expressing P-gp with 17.5% (0.1  $\mu$ M), 10.0% (1  $\mu$ M), and 5.8% (10  $\mu$ M) reduction respectively (Fig. 5b). Similar to densitometry analysis, rifampicin increased the percentage of cells expressing P-gp (41.7%), meanwhile quinidine significantly reduced the percentage of cells expressing P-gp (4.2%) in the apical surface of Caco-2 cells respectively. Figure 6 shows the representative images for the view of the z stack section of cells treated with 0.1–10  $\mu$ M of mitragynine and control drugs.

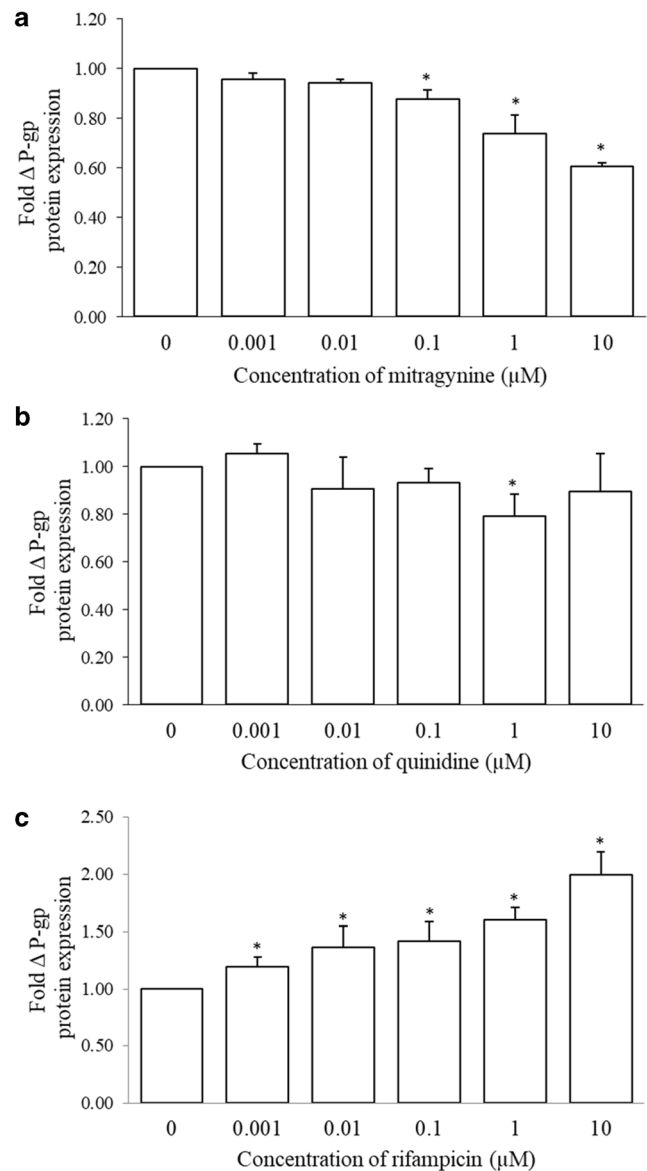


**Fig. 4** The effects of **a** mitragynine, **b** quinidine, and **c** rifampicin on the protein expression of P-gp after 72 h of treatment. Densitometric data of upper bands are presented as mean  $\pm$  SD of three independent experiments ( $n = 3$ , \* $p \leq 0.05$ )

## Discussion

Kratom preparations have been used as a folk remedy among rural population of Malaysia and Thailand (Adkins et al. 2011; Hassan et al. 2013). Due to its stimulant and euphoric effects, kratom is often being misused. In addition to causing symptoms of addiction, kratom is also reported to have effects on the health, psychological, and cognitive behavior of users (Saingam et al. 2013). A cross-sectional survey in the community across three northern peninsular states of Malaysia revealed that regular users of kratom are often afflicted with drug dependence, development of withdrawal symptoms, and inability to control craving (Singh et al. 2014). A number of

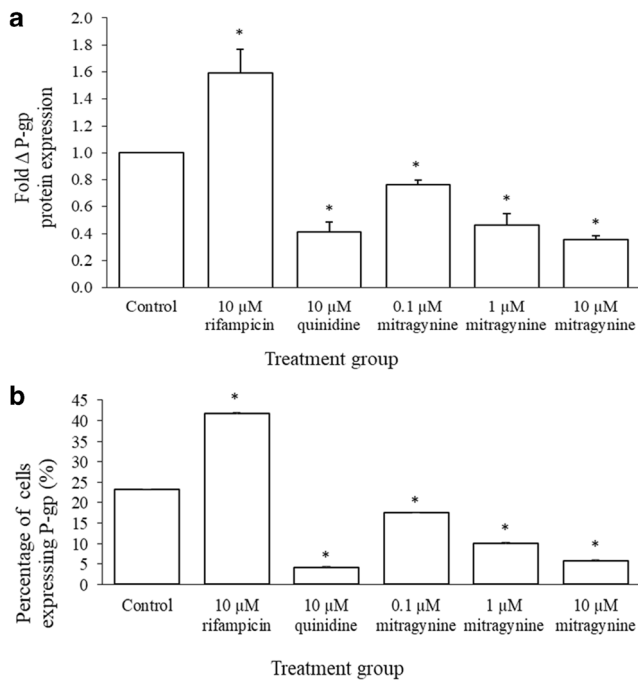


**Fig. 5** **a** The integrated density of the fluorescence signal relative to control or fold changes of P-gp expression in the absence and presence of test compounds. **b** The mean percentage of cells expressing green fluorescence per spot of an approximate 100 cells. Data are presented as mean  $\pm$  SD of three independent experiments ( $n = 3$ ,  $*p \leq 0.05$ )

clinical cases on kratom use related to the development of severe toxicity leading to seizure, coma, and even death have been reported. Most of these cases involved co-administration of at least one additional psychoactive drug, namely, zopiclone, citalopram, lamotrigine, modafinil, benzodiazepine, and quetiapine (Boyer et al. 2008; Hughes 2018; Karinen et al. 2014; Neerman et al. 2013; Tatum et al. 2018). Other than prescription drugs, co-administration of kratom with herb such as *Datura stramonium*, which caused a series of seizure and coma was also reported (Nelsen et al. 2010). Since mitragynine was detected concurrently with other drugs during forensic analysis, these clinical cases have raised serious concern regarding the safety of kratom preparation and the possibility for this major psychoactive component causing serious drug interactions.

In a recent work, mitragynine was found to induce mRNA and protein expression of CYP1A2 but appeared to be a weak CYP3A4 inducer at the transcriptional level and a weak CYP3A4 enzyme inhibitor (Lim et al. 2013). However, in another study, methanolic extract of kratom leaves and several of its alkaloids were found to activate PXR and to induce the mRNA expression of PXR target genes such as CYP3A4, CYP1A2, and P-gp in HepG2 cells, suggesting possible clinically significant drug-herb interactions when used concomitantly with substrate drugs (Manda et al. 2017). The variability of the results may be due to the different methods used; hence, more studies should be carried out to verify this.

Among all transporters, P-gp plays a critical role in drug interactions due to its broad substrate specificity and potential to impact oral bioavailability of substrate drugs. The emerging of many new P-gp substrates and/or inhibitors among active compounds derived from medicinal plant suggests that drug-herb interactions related to P-gp may occur frequently and screening of these phytochemicals against drug interactions risks mediated by P-gp is important (Kivistö et al. 2004; König et al. 2013; Li et al. 2015; Yang et al. 2013). Mitragynine, a bioactive alkaloid of kratom extract is responsible for most of the plant's pharmacological activities. Despite its popularity among illicit drug users, most of the pharmacological studies and scientific evidences only focus on its medicinal potential such as anti-nociceptive, anti-inflammatory, and gastrointestinal effects but its drug-herb interactions risks remain largely uncertain (Hassan et al. 2013; Utar et al. 2011).

In this study, an in silico prediction was first explored to evaluate if mitragynine behaves like a substrate and/or inhibitor of P-glycoprotein. Molecular docking is one of the most frequently used methods because of its ability to predict, with a substantial degree of accuracy, the conformation of small molecule ligands within the appropriate target binding site of macromolecule (Ferreira et al. 2015). The crystal structure of mouse P-gp (PDB: 4KSB) used in this study has 87% similarity on the overall sequence identity and nearly 100% identity within the binding cavity between mouse and human P-gp (Dolghih et al. 2011). In P-gp, the binding sites for transporting substrates (drug binding sites) are formed by interaction of several transmembrane helices, making a pore for the substrate to pass through before being transported to the extracellular space upon ATP hydrolysis (Wise 2012). Thus, for the evaluation of mitragynine as a P-gp substrate, the grid parameter for docking simulation was set to include the substrate binding site. Based on the FEB and  $K_i$  values computed using the docking software, mitragynine was postulated to be either a much weaker P-gp substrate or a non-substrate as compared with digoxin. Both FEB and  $K_i$  values for mitragynine were consistently higher than digoxin. None of the hydrogen and hydrophobic interactions between mitragynine and P-gp residues was similar to digoxin. By contrast, digoxin was shown to form hydrogen bond with Tyr303, one of the important substrate binding sites of P-gp. Tyr303 residue is also known to interact with verapamil, another known P-gp substrate (Yang et al. 2013). These in silico observations on mitragynine were further supported with the bidirectional assay results. Mitragynine has poor permeability and produced an ER value of less than 2; thus, it is unlikely a P-gp substrate. This observation was also similar to the work carried out by Manda and co-workers (Manda et al. 2014). Both mitragynine and 7-hydroxymitragynine were found to have moderate permeability across Caco-2 and MDR-MDCK monolayers with no significant efflux.

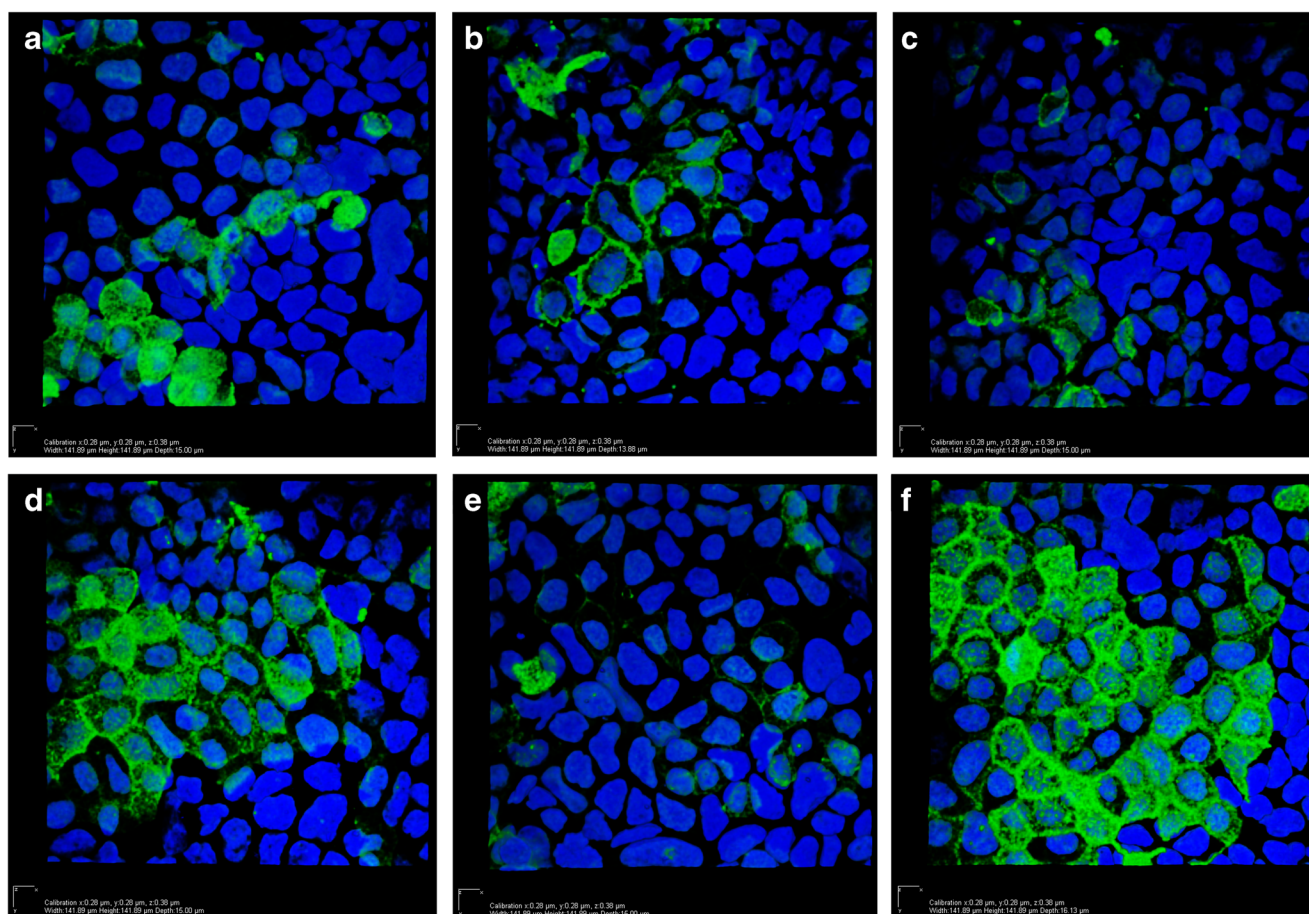


**Fig. 6** Confocal microscope images from representative slides of Caco-2 cells treated with **a** 0.1  $\mu\text{M}$  mitragynine, **b** 1  $\mu\text{M}$  mitragynine, **c** 10  $\mu\text{M}$  mitragynine, **d** 0.1% (v/v) DMSO, **e** 10  $\mu\text{M}$  quinidine, and **f** 10  $\mu\text{M}$

rifampicin (magnification, 63 $\times$  objective). Green fluorescence represents P-gp distribution and expression in Caco-2 cells while blue fluorescence indicates the nucleus

Compounds that interfere with nucleotide binding to P-gp or that disrupt the nucleotide binding sites may inhibit ATP binding or hydrolysis, and hence, in this study, the grid parameter was also set to include the nucleotide binding domain (NBD) of P-gp (Brewer et al. 2014). In this study, although the FEB and  $K_i$  values for mitragynine were slightly lower than quinidine, both compounds exhibited similar interactions with important residues. For example, mitragynine forms three hydrogen bonds with Arg258, an important residue of the P-gp nucleotide binding site as compared with quinidine, which forms a single hydrogen bond with the same residue. In addition, mitragynine interacts with alkyl group of the Pro803 residue via both hydrogen bond and hydrophobic interactions, whereas quinidine interacts with the alkyl group of Pro803 via hydrophobic interactions, suggesting that mitragynine is likely to bind onto the same nucleotide binding site like quinidine. Most of the interactions form by both mitragynine and quinidine were with the important residues in the NBD of P-gp namely Arg258, Phe800, Asp801, Asn805, Tyr1040, and Gln1077 (Brewer et al. 2014). Binding of any xenobiotic into the NBD of P-gp or other ATPase transporters are known to

inhibit ATPase activity and thus preventing the transportation of the substrate (Badhan and Penny 2006). Based on the in silico prediction, mitragynine is likely a P-gp inhibitor and this was further supported by the experimental results and was in agreement with another published study (Manda et al. 2014).

In this study, bidirectional transport assay utilizing Caco-2 cell line was used to evaluate if mitragynine is a P-gp substrate and/or inhibitor. The bidirectional transport assay was first validated by monitoring the transport activity of digoxin through the monolayer cells with and without the present of quinidine, a known P-gp inhibitor. Drug with net efflux ratio more or equal to 2.0 and where its net efflux ratio is influenced by any known P-gp inhibitors is most probably a P-gp substrate (FDA 2012). A high efflux ratio of  $P_{app\ BL-AP}$  to  $P_{app\ AP-BL}$  of digoxin indicates a potentially significant role for P-gp in transporting digoxin across the monolayer cells (Meyer et al. 2015). Low  $P_{app\ AP-BL}$  also reflects an involvement of P-gp in limiting the absorption of the drugs as P-gp was localized on the apical surface of the Caco-2 cells (Artursson et al. 2012). In the presence of quinidine, a reduction in the  $P_{app\ BL-AP}$  resulted in the reduction of the net efflux ratio, indicating an



inhibition on the P-gp transport activity of digoxin and functionality of the bidirectional assay. For evaluation of mitragynine as P-gp inhibitor, the transport of digoxin across the monolayer cell with and without mitragynine and control drug was determined. In this study, the transport of digoxin decreased with increasing concentration of mitragynine and concentration at 10  $\mu\text{M}$  produced a significant reduction of ER (30%) and  $P_{\text{app BL-AP}}$  values, suggesting that mitragynine is a P-gp inhibitor, rather similar to quinidine (40% reduction at 10  $\mu\text{M}$ ). In this study, the actual  $\text{IC}_{50}$  value of mitragynine was not determined, as concentrations above 10  $\mu\text{M}$  may be detrimental to the growth of Caco-2 cells. However, we hypothesized that the  $\text{IC}_{50}$  value for mitragynine would be above 10  $\mu\text{M}$  and that the  $[I]_2/\text{IC}_{50}$  value for mitragynine would be more than 25 if  $[I]_2$  value (inhibitor gut concentration) for mitragynine is approximated at 25 mg in 250 mL (Fenner et al. 2009; Vicknasingam et al. 2010).  $[I]_2/\text{IC}_{50} < 10$  is predictive of negative clinical digoxin DDIs (Fenner et al. 2009); hence, further clinical study is recommended for mitragynine.

Meyer and co-workers evaluated the effects of various psychoactive substances on P-gp and ATPase activity by monitoring transport across cell monolayers and ATP consumption. They found that although mitragynine has demonstrated low ATP consumption, it was capable of inhibiting the P-gp activity in a significant manner, an observation which was similar to our findings (Meyer et al. 2015). In this study, mitragynine was also found to inhibit the mRNA and protein expression of P-gp which further provides information on the possible involvement of this transporter in intestinal absorption and excretion of kratom. A pre- and post-transcriptional reduction of the P-gp expression and binding onto the NBD site may explain the synergistic reduction of P-gp transport activity by mitragynine. However, it is also noteworthy that the reduction of P-gp expression in this case may be also due to other factors such as the cytotoxicity effects of the compound or when the cells were manipulated under reduced serum concentrations. Interestingly, in some cancer cells, a decreased P-gp turnover (increased stability) is closely associated with the G1/G0 phase of the cell cycle and when the cells are placed under some physiological stress such as serum starvation, amino acid deficiency, or radiation treatment (Zhang and Ling 2000). Apparently, under serum-starved conditions, there is an enhanced degradation of total cytoplasmic and membrane proteins and that the steady-state level of P-gp in a cell is dependent on its synthesis rate and turnover rate (Zhang and Ling 2000). Interestingly, in another study, treatment with *Mitragyna* extract and its constituent such as mitragynine resulted in increased in both PXR and P-gp expression. This was followed by a decreased in the uptake of Calcein-AM in HepG2 cells, suggesting an increased P-gp activity (Manda et al. 2017). This discrepancy may be due to the different cell lines, assay conditions and substrates used in the experiments. In addition, there is also a limitation with the current method

using HPLC system, namely, sensitivity issue, which can be improved with UPLC or LC/MS-MS system.

Interestingly, from the immunocytochemistry results, mitragynine significantly inhibited the surface expression of P-gp in Caco-2 cells at lower concentrations of 0.1  $\mu\text{M}$  and onwards. P-gp is first synthesized in the endoplasmic reticulum (ER) as a core-glycosylated intermediate with a molecular mass of about 150 kDa before subsequently modified in the Golgi apparatus and transported to the cell membrane (Grandjean-Forestier et al. 2009). Thus, a reduction in surface expression suggests that mitragynine may possibly affect the transportation and trafficking of P-gp from the endoplasmic reticulum (ER) to the apical surface of the Caco-2 cells. However, further work would be required to prove this point.

Other than mitragynine, rifampicin and quinidine were also evaluated in both bidirectional assay and molecular studies. As expected, the transport activity of P-gp was significantly induced by rifampicin and this was in agreement with its total protein expression and surface localization, and the findings were similar with a published study (Haslam et al. 2008). Meanwhile, quinidine was found to significantly inhibit the P-gp transport activity as well as the expression of P-gp at both transcriptional and translational level. In addition, quinidine also showed a significant inhibition on P-gp surface expression at 10  $\mu\text{M}$  and further suggests that the overall transport inhibition activity does not solely rely on direct compound binding alone and these findings were unreported previously. Quinidine and digoxin are both substrates for P-glycoprotein and quinidine is a potent inhibitor of digoxin transport in vitro (Fromm et al. 1999). Quinidine is a weak inhibitor of CYP3A but a strong inhibitor of P-gp (Bui et al. 2016). Interestingly, mitragynine is known to be a weak CYP3A4 inhibitor and also proved to be a significant P-gp inhibitor comparable to quinidine.

In conclusion, mitragynine inhibits the P-gp transport activity in vitro probably via binding onto the NBD site of P-gp molecule and by inhibiting the mRNA and protein expression P-gp in the Caco-2 cells. However, its effects on the P-gp trafficking pathway to the Caco-2 membrane require further investigation. Concurrent administration of kratom products with psychoactive drugs which are P-gp substrates may probably lead to clinically significant toxicity. Further clinical study to prove this point is needed.

**Acknowledgements** The authors would like to acknowledge MyBrain15 program and USM fellowship for sponsoring NR.

**Author contribution statement** TML, MIA, GK, and SFS conceived and designed research. NR and AA conducted experiments. HAW contributed analytical tools for in silico screening. TML and NR analyzed data. TML wrote the manuscript. All authors read and approved the manuscript.

**Funding** This fundamental work was supported in parts by the Fundamental Research Grant Scheme (Ministry of Education Malaysia) and RUI (USM) grant awarded to TML.

**Compliance with ethical standards** No animals or human were used in this study.

**Conflict of interest** The authors declare that they have no conflict of interests.

**Publisher's Note** Springer Nature remains neutral with regard to jurisdictional claims in published maps and institutional affiliations.

## References

- Adkins JE, Boyer EW, McCurdy CR (2011) *Mitragyna speciosa*, a psychoactive tree from Southeast Asia with opioid activity. *Curr Top Med Chem* 11:1165–1175. <https://doi.org/10.2174/156802611795371305>
- Ahmad K, Aziz Z (2012) *Mitragyna speciosa* use in the northern states of Malaysia: a cross-sectional study. *J Ethnopharmacol* 141:446–450. <https://doi.org/10.1016/j.jep.2012.03.009>
- Artursson P, Palm K, Luthman K (2012) Caco-2 monolayers in experimental and theoretical predictions of drug transport. *Adv Drug Deliv Rev* 64(Supplement):280–289. <https://doi.org/10.1016/j.addr.2012.09.005>
- Aszalos A (2007) Drug-drug interactions affected by the transporter protein, P-glycoprotein (ABCB1, MDR1) II. Clinical aspects. *Drug Discov Today* 12:838–843. <https://doi.org/10.1016/j.drudis.2007.07.021>
- Badhan R, Penny J (2006) In silico modelling of the interaction of flavonoids with human P-glycoprotein nucleotide-binding domain. *Eur J Med Chem* 41:285–295. <https://doi.org/10.1016/j.ejmech.2005.11.012>
- Borst P, Elferink RO (2002) Mammalian ABC transporters in health and disease. *Annu Rev Biochem* 71:537–592. <https://doi.org/10.1146/annurev.biochem.71.102301.093055>
- Boyer EW, Babu KM, Adkins JE, McCurdy CR, Halpern JH (2008) Self-treatment of opioid withdrawal using kratom (*Mitragyna speciosa* Korth). *Addiction* 103:1048–1050. <https://doi.org/10.1111/j.1360-0443.2008.02209.x>
- Brewer FK, Follit CA, Vogel PD, Wise JG (2014) In silico screening for inhibitors of P-glycoprotein that target the nucleotide binding domains. *Mol Pharmacol* 86:716–726. <https://doi.org/10.1124/mol.114.095414>
- Bui K, She F, Zhou D, Butler K, Al-Humiti N, Sostek M (2016) The effect of quinidine, a strong P-glycoprotein inhibitor, on the pharmacokinetics and central nervous system distribution of naloxegol. *J Clin Pharmacol* 56:497–505. <https://doi.org/10.1002/jcph.613>
- Chittrakarn S, Keawpradub N, Sawangjareon K, Kansanalak S, Janchawee B (2010) The neuromuscular blockade produced by pure alkaloid, mitragynine and methanol extract of kratom leaves (*Mitragyna speciosa* Korth.). *J Ethnopharmacol* 129:344–349. <https://doi.org/10.1016/j.jep.2010.03.035>
- Dolghih E, Bryant C, Renslo AR, Jacobson MP (2011) Predicting binding to P-glycoprotein by flexible receptor docking. *PLoS Comput Biol* 7:e1002083. <https://doi.org/10.1371/journal.pcbi.1002083>
- Domingo O, Roeder G, Stover A, Graw M, Musshoff F, Sachs H, Bicker W (2017) Mitragynine concentrations in two fatalities. *Forensic Sci Int* 271:e1–e7. <https://doi.org/10.1016/j.forsciint.2016.12.020>
- FDA (2012) Guidance for industry—drug interaction studies—study design, data analysis, implications for dosing, and labeling recommendations. Center for Drug Evaluation and Research, Food and Drug Administration, Rockville
- Fenner KS, Troutman MD, Kempshall S, Cook JA, Ware JA, Smith DA, Lee CA (2009) Drug–drug interactions mediated through P-glycoprotein: clinical relevance and in vitro–in vivo correlation using digoxin as a probe drug. *Clin Pharmacol Ther* 85:173–181. <https://doi.org/10.1038/clpt.2008.195>
- Ferreira LG, Dos Santos RN, Oliva G, Andricopulo AD (2015) Molecular docking and structure-based drug design strategies. *Molecules* 20:13384–13421. <https://doi.org/10.3390/molecules200713384>
- Ferruzza S, Rossi C, Scarino ML, Sambuy Y (2012) A protocol for differentiation of human intestinal Caco-2 cells in asymmetric serum-containing medium. *Toxicol in Vitro* 26:1252–1255. <https://doi.org/10.1016/j.tiv.2012.01.008>
- Fromm MF, Kim RB, Stein CM, Wilkinson GR, Roden DM (1999) Inhibition of P-glycoprotein-mediated drug transport: a unifying mechanism to explain the interaction between digoxin and quinidine [see comments]. *Circulation* 99:552–557
- Grandjean-Forestier F, Stenger C, Robert J, Verdier M, Ratinaud M-H (2009) The P-glycoprotein 170: just a multidrug resistance protein or a protean molecule? In: ABC transporters and multidrug resistance. John Wiley & Sons, Inc., pp 15–46. doi:<https://doi.org/10.1002/9780470495131.ch1>
- Grundmann O (2017) Patterns of kratom use and health impact in the US—results from an online survey. *Drug Alcohol Depend* 176:63–70. <https://doi.org/10.1016/j.drugalcdep.2017.03.007>
- Haslam IS, Jones K, Coleman T, Simmons NL (2008) Induction of P-glycoprotein expression and function in human intestinal epithelial cells (T84). *Biochem Pharmacol* 76:850–861. <https://doi.org/10.1016/j.bcp.2008.07.020>
- Hassan Z, Muzaimi M, Navaratnam V, Yusoff NHM, Suhaimi FW, Vadivelu R, Vicknasingam BK, Amato D, von Hörsten S, Ismail NIW, Jayabalan N, Hazim AI, Mansor SM, Müller CP (2013) From kratom to mitragynine and its derivatives: physiological and behavioural effects related to use, abuse, and addiction. *Neurosci Biobehav Rev* 37:138–151. <https://doi.org/10.1016/j.neubiorev.2012.11.012>
- Hennessy M, Spiers JP (2007) A primer on the mechanics of P-glycoprotein the multidrug transporter. *Pharmacol Res* 55:1–15. <https://doi.org/10.1016/j.phrs.2006.10.007>
- Henningfield JE, Fant RV, Wang DW (2018) The abuse potential of kratom according to the 8 factors of the controlled substances act: implications for regulation and research. *Psychopharmacology* 235:573–589. <https://doi.org/10.1007/s00213-017-4813-4>
- Hillebrand J, Olszewski D, Sedefov R (2010) Legal highs on the internet. *Subst Use Misuse* 45:330–340. <https://doi.org/10.3109/10826080903443628>
- Hughes RL (2018) Fatal combination of mitragynine and quetiapine—a case report with discussion of a potential herb–drug interaction. *Forensic Sci Med Pathol*. <https://doi.org/10.1007/s12024-018-0049-9>
- Jamil MFA, Subki MFM, Lan TM, Majid MIA, Adenan MI (2013) The effect of mitragynine on cAMP formation and mRNA expression of mu-opioid receptors mediated by chronic morphine treatment in SK–N–SH neuroblastoma cell. *J Ethnopharmacol* 148:135–143. <https://doi.org/10.1016/j.jep.2013.03.078>
- Janchawee B, Keawpradub N, Chittrakarn S, Praseththo S, Wararatnanurak P, Sawangjareon K (2007) A high-performance liquid chromatographic method for determination of mitragynine in serum and its application to a pharmacokinetic study in rats. *Biomed Chromatogr* 21:176–183. <https://doi.org/10.1002/bmc.731>
- Jedlička A, Grafnetterová T, Miller V (2003) HPLC method with UV detection for evaluation of digoxin tablet dissolution in acidic medium after solid-phase extraction. *J Pharm Biomed Anal* 33:109–115. [https://doi.org/10.1016/S0731-7085\(03\)00226-7](https://doi.org/10.1016/S0731-7085(03)00226-7)
- Kapp FG, Maurer HH, Auwarter V, Winkelmann M, Hermanns-Clausen M (2011) Intrahepatic cholestasis following abuse of powdered kratom (*Mitragyna speciosa*). *J Med Toxicol* 7:227–231. <https://doi.org/10.1007/s13181-011-0155-5>

- Karinen R, Fosen JT, Rogde S, Vindenes V (2014) An accidental poisoning with mitragynine. *Forensic Sci Int* 245C:e29–e32. <https://doi.org/10.1016/j.forsciint.2014.10.025>
- Kivistö KT, Niemi M, Fromm MF (2004) Functional interaction of intestinal CYP3A4 and P-glycoprotein. *Fundam Clin Pharmacol* 18: 621–626. <https://doi.org/10.1111/j.1472-8206.2004.00291.x>
- Kong WM, Chik Z, Ramachandra M, Subramaniam U, Aziddin RE, Mohamed Z (2011) Evaluation of the effects of *Mitragyna speciosa* alkaloid extract on cytochrome P450 enzymes using a high throughput assay. *Molecules* 16:7344–7356. <https://doi.org/10.3390/molecules16097344>
- König J, Müller F, Fromm MF (2013) Transporters and drug-drug interactions: important determinants of drug disposition and effects. *Pharmacol Rev* 65:944–966. <https://doi.org/10.1124/pr.113.007518>
- Kronstrand R, Roman M, Thelander G, Eriksson A (2011) Unintentional fatal intoxications with mitragynine and O-desmethyltramadol from the herbal blend Krypton. *J Anal Toxicol* 35:242–247
- Li M, de Graaf IAM, de Jager MH, Groothuis GMM (2015) Rat precision-cut intestinal slices to study P-gp activity and the potency of its inhibitors ex vivo. *Toxicol in Vitro* 29:1070–1078. <https://doi.org/10.1016/j.tiv.2015.04.011>
- Lim EL, Seah TC, Koe XF, Wahab HA, Adenan MI, Jamil MFA, Majid MIA, Tan ML (2013) In vitro evaluation of cytochrome P450 induction and the inhibition potential of mitragynine, a stimulant alkaloid. *Toxicol in Vitro* 27:812–824. <https://doi.org/10.1016/j.tiv.2012.12.014>
- Lu J, Wei H, Wu J, Jamil MFA, Tan ML, Adenan MI, Wong P, Shim W (2014) Evaluation of the cardiotoxicity of mitragynine and its analogues using human induced pluripotent stem cell-derived cardiomyocytes. *PLoS One* 9:e115648. <https://doi.org/10.1371/journal.pone.0115648>
- Manda VK, Avula B, Ali Z, Khan IA, Walker LA, Khan SI (2014) Evaluation of in vitro absorption, distribution, metabolism, and excretion (ADME) properties of mitragynine, 7-hydroxymitragynine, and mitraphylline. *Planta Med* 80:568–576. <https://doi.org/10.1055/s-0034-1368444>
- Manda VK, Avula B, Dale OR, Ali Z, Khan IA, Walker LA, Khan SI (2017) PXR mediated induction of CYP3A4, CYP1A2, and P-gp by *Mitragyna speciosa* and its alkaloids. *Phytother Res* 31:1935–1945. <https://doi.org/10.1002/ptr.5942>
- Matsumoto K, Mizowaki M, Suchitra T, Murakami Y, Takayama H, Sakai SI, Aimi N, Watanabe H (1996a) Central antinociceptive effects of mitragynine in mice: contribution of descending noradrenergic and serotonergic systems. *Eur J Pharmacol* 317:75–81
- Matsumoto K, Mizowaki M, Suchitra T, Takayama H, Sakai S, Aimi N, Watanabe H (1996b) Antinociceptive action of mitragynine in mice: evidence for the involvement of supraspinal opioid receptors. *Life Sci* 59:1149–1155. [https://doi.org/10.1016/0024-3205\(96\)00432-8](https://doi.org/10.1016/0024-3205(96)00432-8)
- Matsumoto K, Horie S, Ishikawa H, Takayama H, Aimi N, Ponglux D, Watanabe K (2004) Antinociceptive effect of 7-hydroxymitragynine in mice: discovery of an orally active opioid analgesic from the Thai medicinal herb *Mitragyna speciosa*. *Life Sci* 74:2143–2155. <https://doi.org/10.1016/j.lfs.2003.09.054>
- Meyer MR, Waggmann L, Schneider-Daum N, Loretz B, de Souza CC, Lehr C-M, Maurer HH (2015) P-glycoprotein interactions of novel psychoactive substances—stimulation of ATP consumption and transport across Caco-2 monolayers. *Biochem Pharmacol* 94:220–226. <https://doi.org/10.1016/j.bcp.2015.01.008>
- Mikkaichi T, Yoshigae Y, Masumoto H, Imaoka T, Rozehnal V, Fischer T, Okudaira N, Izumi T (2014) Edoxaban transport via P-glycoprotein is a key factor for the drug's disposition. *Drug Metab Dispos* 42: 520–528. <https://doi.org/10.1124/dmd.113.054866>
- Montanari F, Ecker GF (2015) Prediction of drug-ABC-transporter interaction—recent advances and future challenges. *Adv Drug Deliv Rev* 86:17–26. <https://doi.org/10.1016/j.addr.2015.03.001>
- Morris GM, Huey R, Lindstrom W, Sanner MF, Belew RK, Goodsell DS, Olson AJ (2009) AutoDock4 and AutoDockTools4: automated docking with selective receptor flexibility. *J Comput Chem* 30: 2785–2791. <https://doi.org/10.1002/jcc.21256>
- Neerman MF, Frost RE, Deking J (2013) A drug fatality involving kratom. *J Forensic Sci* 58(Suppl 1):S278–S279. <https://doi.org/10.1111/1556-4029.12009>
- Nelsen JL, Lapoint J, Hodgman MJ, Aldous KM (2010) Seizure and coma following kratom (*Mitragyna speciosa* Korth) exposure. *J Med Toxicol* 6:424–426. <https://doi.org/10.1007/s13181-010-0079-5>
- Oga EF, Sekine S, Shitara Y, Horie T (2012) P-glycoprotein mediated efflux in Caco-2 cell monolayers: the influence of herbals on digoxin transport. *J Ethnopharmacol* 144:612–617. <https://doi.org/10.1016/j.jep.2012.10.001>
- Pan X, Mei H, Qu S, Huang S, Sun J, Yang L, Chen H (2016) Prediction and characterization of P-glycoprotein substrates potentially bound to different sites by emerging chemical pattern and hierarchical cluster analysis. *Int J Pharm* 502:61–69. <https://doi.org/10.1016/j.ijpharm.2016.02.022>
- Peng Y, Yadava P, Heikkinen AT, Parrott N, Railkar A (2014) Applications of a 7-day Caco-2 cell model in drug discovery and development. *Eur J Pharm Sci* 56:120–130. <https://doi.org/10.1016/j.ejps.2014.02.008>
- Philipp AA, Wissenbach DK, Weber AA, Zapp J, Maurer HH (2011) Metabolism studies of the kratom alkaloids mitraciliatine and isopaynantheine, diastereomers of the main alkaloids mitragynine and paynantheine, in rat and human urine using liquid chromatography-linear ion trap-mass spectrometry. *J Chromatogr B Analyt Technol Biomed Life Sci* 879:1049–1055. <https://doi.org/10.1016/j.jchromb.2011.03.005>
- Saingan D, Assanangkornchai S, Geater AF, Balthip Q (2013) Pattern and consequences of kratom (*Mitragyna speciosa* Korth.) use among male villagers in southern Thailand: a qualitative study. *Int J Drug Policy* 24:351–358. <https://doi.org/10.1016/j.drugpo.2012.09.004>
- Schmidt MM, Sharma A, Schifano F, Feinmann C (2011) “Legal highs” on the net—evaluation of UK-based websites, products and product information. *Forensic Sci Int* 206:92–97. <https://doi.org/10.1016/j.forsciint.2010.06.030>
- Singh D, Muller CP, Vicknasingam BK (2014) Kratom (*Mitragyna speciosa*) dependence, withdrawal symptoms and craving in regular users. *Drug Alcohol Depend* 139:132–137. <https://doi.org/10.1016/j.drugalcdep.2014.03.017>
- Srinivasan B, Kolli AR, Esch MB, Abaci HE, Shuler ML, Hickman JJ (2015) TEER measurement techniques for in vitro barrier model systems. *J Lab Autom* 20:107–126. <https://doi.org/10.1177/2211068214561025>
- Swogger MT, Hart E, Erowid F, Erowid E, Trabold N, Yee K, Parkhurst KA, Priddy BM, Walsh Z (2015) Experiences of kratom users: a qualitative analysis. *J Psychoactive Drugs* 47:360–367. <https://doi.org/10.1080/02791072.2015.1096434>
- Szakacs G, Paterson JK, Ludwig JA, Booth-Genthe C, Gottesman MM (2006) Targeting multidrug resistance in cancer. *Nat Rev Drug Discov* 5:219–234. <https://doi.org/10.1038/nrd1984>
- Tachibana T, Kato M, Takano J, Sugiyama Y (2010) Predicting drug-drug interactions involving the inhibition of intestinal CYP3A4 and P-glycoprotein. *Curr Drug Metab* 11:762–777. <https://doi.org/10.2174/138920010794328922>
- Tan HK, Muhammad TST, Tan ML (2016) 14-Deoxy-11,12-didehydroandrographolide induces DDIT3-dependent endoplasmic reticulum stress-mediated autophagy in T-47D breast carcinoma cells. *Toxicol Appl Pharmacol* 300:55–69. <https://doi.org/10.1016/j.taap.2016.03.017>
- Tatum WO, Hasan TF, Coonan EE, Smelick CP (2018) Recurrent seizures from chronic kratom use, an atypical herbal opioid. *Epilepsy Behav Case Rep* 10:18–20. <https://doi.org/10.1016/j.ebcr.2018.04.002>

- Tay YL, Teah YF, Chong YM, Jamil MFA, Kollert S, Adenan MI, Wahab HA, Döring F, Wischmeyer E, Tan ML (2016) Mitragynine and its potential blocking effects on specific cardiac potassium channels. *Toxicol Appl Pharmacol* 305:22–39. <https://doi.org/10.1016/j.taap.2016.05.022>
- Thongpradichote S, Matsumoto K, Tohda M, Takayama H, Aimi N, Sakai S, Watanabe H (1998) Identification of opioid receptor subtypes in antinociceptive actions of supraspinally-administered mitragynine in mice. *Life Sci* 62:1371–1378
- Utar Z, Majid MIA, Adenan MI, Jamil MFA, Lan TM (2011) Mitragynine inhibits the COX-2 mRNA expression and prostaglandin E2 production induced by lipopolysaccharide in RAW264.7 macrophage cells. *J Ethnopharmacol* 136:75–82. <https://doi.org/10.1016/j.jep.2011.04.011>
- Vaalburg W, Hendrikse NH, Elsinga PH, Bart J, van Waarde A (2005) P-glycoprotein activity and biological response. *Toxicol Appl Pharmacol* 207:257–260. <https://doi.org/10.1016/j.taap.2005.03.027>
- Varma MVS, Kapoor N, Sarkar M, Panchagnula R (2004) Simultaneous determination of digoxin and permeability markers in rat in situ intestinal perfusion samples by RP-HPLC. *J Chromatogr B* 813:347–352. <https://doi.org/10.1016/j.jchromb.2004.09.047>
- Vicknasingam B, Narayanan S, Beng GT, Mansor SM (2010) The informal use of ketum (*Mitragyna speciosa*) for opioid withdrawal in the northern states of peninsular Malaysia and implications for drug substitution therapy. *Int J Drug Policy* 21:283–288. <https://doi.org/10.1016/j.drugpo.2009.12.003>
- Wang Q, Strab R, Kardos P, Ferguson C, Li J, Owen A, Hidalgo IJ (2008) Application and limitation of inhibitors in drug-transporter interactions studies. *Int J Pharm* 356:12–18. <https://doi.org/10.1016/j.ijpharm.2007.12.024>
- Ward AB, Szewczyk P, Grimard V, Lee CW, Martinez L, Doshi R, Caya A, Villaluz M, Pardon E, Cregger C, Swartz DJ, Falson PG, Urbatsch IL, Govaerts C, Steyaert J, Chang G (2013) Structures of P-glycoprotein reveal its conformational flexibility and an epitope on the nucleotide-binding domain. *Proc Natl Acad Sci U S A* 110:13386–13391. <https://doi.org/10.1073/pnas.1309275110>
- White CM (2018) Pharmacologic and clinical assessment of kratom. *Am J Health Syst Pharm* 75:261–267. <https://doi.org/10.2146/ajhp161035>
- Wise JG (2012) Catalytic transitions in the human MDR1 P-glycoprotein drug binding sites. *Biochemistry* 51:5125–5141. <https://doi.org/10.1021/bi300299z>
- Yang C, Zhang T, Li Z, Xu L, Liu F, Ruan J, Liu K, Zhang Z (2013) P-glycoprotein is responsible for the poor intestinal absorption and low toxicity of oral aconitine: in vitro, in situ, in vivo and in silico studies. *Toxicol Appl Pharmacol* 273:561–568. <https://doi.org/10.1016/j.taap.2013.09.030>
- Zhang W, Ling V (2000) Cell-cycle-dependent turnover of P-glycoprotein in multidrug-resistant cells. *J Cell Physiol* 184:17–26. [https://doi.org/10.1002/\(SICI\)1097-4652\(200007\)184:1<17::AID-JCP2>3.0.CO;2-U](https://doi.org/10.1002/(SICI)1097-4652(200007)184:1<17::AID-JCP2>3.0.CO;2-U)